APL Materials

RESEARCH ARTICLE | MAY 01 2023

Epitaxial hexagonal boron nitride with high quantum efficiency

David Arto Laleyan ; Woncheol Lee ; Ying Zhao ; Yuanpeng Wu ; Ping Wang ; Jun Song ; Emmanouil Kioupakis ; Zetian Mi

APL Mater. 11, 051103 (2023)
https://doi.org/10.1063/5.0142242

Epitaxial hexagonal boron nitride with high quantum efficiency

Cite as: APL Mater. 11, 051103 (2023); doi: 10.1063/5.0142242
Submitted: 12 January 2023 • Accepted: 7 April 2023 •
Published Online: 1 May 2023

David Arto Laleyan,[1] Woncheol Lee,[1] Ying Zhao,[2] Yuanpeng Wu,[1] Ping Wang,[1] Jun Song,[2,a)] Emmanouil Kioupakis,[3,a)] and Zetian Mi[1,a)]

AFFILIATIONS

[1]Department of Electrical Engineering and Computer Science, University of Michigan, Ann Arbor, Michigan 48109, USA
[2]Department of Materials Engineering, McGill University, Montreal, Quebec H3A 0C5, Canada
[3]Department of Materials Science and Engineering, University of Michigan, Ann Arbor, Michigan 48109, USA

[a)]**Authors to whom correspondence should be addressed:** jun.song2@mcgill.ca; kioup@umich.edu; and ztmi@umich.edu

ABSTRACT

Two-dimensional (2D) hexagonal boron nitride (h-BN) is one of the few materials showing great promise for light emission in the far ultraviolet (UV)-C wavelength, which is more effective and safer in containing the transmission of microbial diseases than traditional UV light. In this report, we observed that h-BN, despite having an indirect energy bandgap, exhibits a remarkably high room-temperature quantum efficienc (~60%), which is orders of magnitude higher than that of other indirect bandgap material, and is enabled by strong excitonic effects and efficien exciton-phonon interactions. This study offers a new approach for the design and development of far UV-C optoelectronic devices as well as quantum photonic devices employing 2D semiconductor active regions.

Hexagonal boron nitride (h-BN) has drawn tremendous attention, given its unique characteristic of being a two-dimensional (2D) quantum material, making it a fundamental building block of van der Waals heterostructures[1] for future nanoscale electronic, photonic, and quantum devices.[2,3] Little attention, however, has been paid to the ultrawide bandgap nature of h-BN, which is ideally suited to form heterostructures with the Al(Ga)N-based semiconductors.[4–6] These semiconductor quantum heterostructures are the material of choice for solid-state ultraviolet (UV) lamps,[7,8] which are the only alternative to replace conventional mercury and xenon lamps for many critical applications including the disinfection and sterilization of infectious diseases such as the severe acute respiratory syndrome coronavirus 2 (SARS-CoV-2).[9] Although conventional germicidal lamps emit at wavelengths (~260 nm) that are hazardous to humans, far UV-C emitters (207–222 nm) do not have sufficien range to penetrate through the outer layer of the eye and skin but retain the germicidal properties to inactivate microbes[10] and can, therefore, operate continuously in public areas. Progress in developing far UV-C light-emitting diodes (LEDs) utilizing conventional Al(Ga)N materials, however, has been severely limited by the transverse magnetic (TM) polarized emission, the strong polarization field and the presence of extensive defects, which lead to an extremely low quantum efficienc and a poor light extraction efficiency

The synthesis of highly crystalline h-BN has been a topic of extensive study,[11,12] as highlighted in Sec. 1 of the supplementary material. Bulk single-crystal growth is mainly achieved either using a high-pressure, high-temperature (HPHT) method[13] or at atmospheric pressure using molten metal solvents such as Ni or Fe.[14,15] In addition, 2D h-BN, due to van der Waals bonding, can be potentially grown as a thin fil on foreign substrates without the formation of dislocations, as outlined in recent publications.[16] h-BN, however, is an indirect bandgap semiconductor like Si.[17] In such indirect bandgap semiconductors, the near band-edge optical transitions involve phonons, thereby resulting in orders of magnitude lower quantum efficienc than direct bandgap semiconductors. Recent studies on luminescence emission of h-BN have been largely limited to defect-related emission, which has only been exploited as a single photon source operating in the visible or near-UV spectrum.[18–21] Although there have been reports of luminescence from near band-edge transitions in h-BN, including cathodoluminescence (CL),[22] photoluminescence (PL),[17,23–25] and most recently electroluminescence (EL),[26] to date, an unresolved fundamental challenge is whether and how an indirect

bandgap semiconductor can be transformed to be an efficien light emitter.

Herein, we have demonstrated, both theoretically and experimentally, that Ni serves as an ideal substrate for h-BN due to the minimal lattice mismatch and optimal interfacial interactions. By exploiting strong excitonic effects and efficien exciton-phonon coupling, it was observed that an indirect bandgap semiconductor such as h-BN can become a high efficienc far UV-C light emitter. The room-temperature internal quantum efficienc (IQE) is measured to be 60% in the far UV-C (~220 nm), which is orders of magnitude higher than that of other indirect bandgap semiconductors. This work not only provides a viable approach for developing far UV-C light sources for safe and energy-efficien ultraviolet sterilization of disease pathogens but also offers a practical approach to the design and development of quantum optoelectronic and electronic devices utilizing the emerging 2D semiconductor materials.

Conventional high-efficienc LEDs can only be realized by growing on single crystalline substrates, such as sapphire, SiC, GaAs, and InP. In this regard, the epitaxy of h-BN on crystalline semiconducting substrates such as sapphire and AlN has been extensively studied.[27–30] We have performed first-principle density functional theory (DFT) calculations of the heterointerface between the monolayer h-BN and various substrates, including sapphire, AlN, SiO_x, as well as Ni and Cu (see Methods). Our results show that besides the minimal lattice mismatch (~0.5%) with h-BN, Ni exhibits an optimal interfacial interaction with h-BN (i.e., adhesion energy, $\beta_{hBN-sub}$, among other studied systems, see Fig. 1(a). Examining Fig. 1(a), we see that different Ni facets show consistently a good interfacial interaction with h-BN without inducing notable distortion in the h-BN structure. In sharp contrast, SiO_2 shows a very weak interaction with h-BN as evidenced by near-zero $\beta_{hBN-sub}$, whereas sapphire and AlN interact very strongly with h-BN, inducing considerable distortion in the h-BN lattice. Consequently, one would expect it to be difficul for h-BN to nucleate and grow on SiO_2, whereas h-BN grown on sapphire is expected to be highly defective. In addition, theoretically evaluating the effect of substrate, we have also investigated the impact of chemical environments on h-BN growth. One notable aspect is vacancy formation, which is of direct implication to the quality of h-BN.[31–33] It is seen from

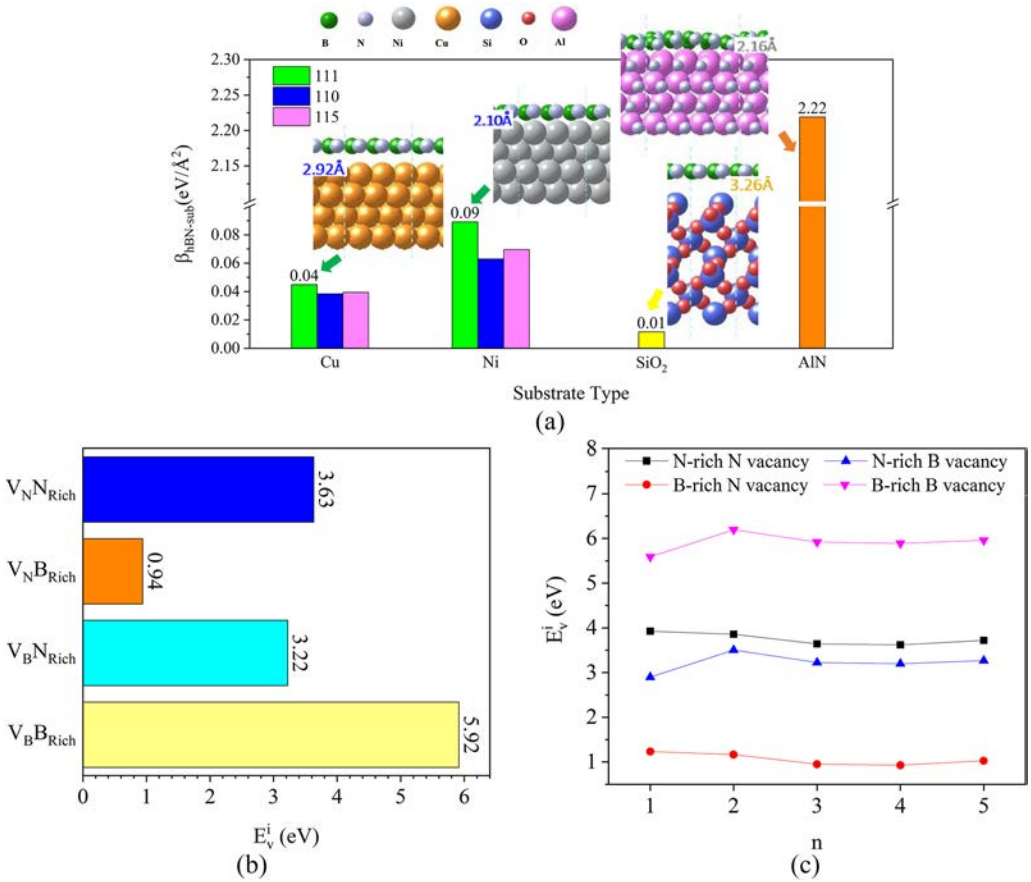

FIG. 1. (a) Interfacial energies for h-BN on different substrates. (b) Boron and nitrogen-vacancy formation energies under boron-rich and nitrogen-rich conditions. (c) The formation energies of B and N vacancies in h-BN supported on the Ni(111) substrate under N-rich and B-rich conditions, computed using a different supercell size *n*. In all vacancy calculations, only one vacancy was created in the supercell.

Fig. 1(b) that under B-rich environments, the formation energy of a N vacancy for substrate-supported h-BN is very small, ~0.94 eV, thereby leading to the presence of extensive N vacancies.[4,34] Under N-rich conditions, however, the formation energies for both B and N vacancies are very large, ~3.5 and 4 eV, respectively. Therefore, one would expect that high-quality h-BN is preferentially grown under N-rich, instead of B-rich, growth conditions.[35–37] Meanwhile, the effect of supercell size on the single vacancy formation energy was also examined, with the results shown in Fig. 1(c), where n corresponds to a supercell of size $n \times n$. We see from Fig. 1(c) that the B vacancy shows the lowest formation energy at the smallest supercell (i.e., $n = 1$), whereas for the N vacancy, its formation energy decreases as the supercell size increases until $n = 3$ and stabilizes for $n > 3$. As the vacancy density is inversely proportional to the supercell size, we can conclude that the B vacancy tends to form at a very high density (i.e., $n = 1$), whereas the N vacancy is more likely to form at lower densities.

Experimentally, we have studied the epitaxy of h-BN on various substrates under N-rich epitaxy conditions (see Methods). It is observed that h-BN grown directly on sapphire and SiO_2 is dominated by defect-related emission across the UV bands, as shown in Sec. 2 of the supplementary material. The epitaxy of h-BN on the Ni substrate, however, exhibits drastically different properties. At room temperature, the PL emission is dominated by deep UV excitonic emission, with suppressed defect-related emission, as predicted by theory. Detailed growth optimization and characterization details are described in Sec. 3 of the supplementary material. The optical properties of the epitaxial h-BN on Ni were further characterized using variable excitation power and temperature-dependent PL spectroscopy, described in Sec. 4 of the supplementary material. The representative PL spectra are shown in Fig. 2(a). At the cryogenic temperature, distinct peaks are resolved at ~220 nm, which are consistent with previous reports of high-quality h-BN as highlighted in the introduction. The quantum efficienc of h-BN deep UV emission is further derived from temperature and power-dependent PL spectroscopy. Based on previous studies of GaN-based LED structures, the highest internal quantum efficienc measured at the cryogenic temperature (e.g., 20 K) is assumed to be unity, due to the suppression of nonradiative recombination.[38–40] The internal quantum efficienc measured at different temperatures and excitation powers can then be obtained by taking the ratio of luminescence efficiency define as the integrated luminescence intensity vs excitation power, with respect to the highest value measured at the cryogenic temperature.[41] It is worth noting that although the optical transition in h-BN is indirect and, therefore, phonon-dependent, which may, in principle, be inefficien at low temperatures, this transition is in fact assisted by phonon emission, which is not sensitive to temperature. Remarkably, as shown in Fig. 2(b), the room-temperature internal quantum efficienc for epitaxial h-BN reaches 60%, which is orders of magnitude higher than that of other indirect bandgap materials and is comparable with, or better than, direct bandgap semiconductors commonly used in commercial LEDs and laser diodes. It is also observed that the efficienc remains relatively constant under low to moderate excitation conditions, which is consistent with the exciton-dominated emission (to be described next). Moreover, the internal quantum efficienc shows a droop with increasing excitation power, which is due to enhanced Auger recombination or other higher-order carrier loss terms under high-excitation conditions. Similar efficienc droop has been commonly measured in GaN-based LEDs.[42–45]

Unlike h-BN, conventional indirect-bandgap semiconductors exhibit extremely low luminescence efficiency preventing their application in LEDs. In this regard, we have performed a detailed theoretical study of the origin of the high luminescence effi ciency of indirect-bandgap h-BN using first-principle calculations (see Methods). First, our band calculations predict an indirect gap of 6.22 eV between the conduction band minimum (CBM) at the M point and the valence band maximum (VBM) close to the K point, shown in Fig. 3(a), which is consistent with previous reports.[23,46–48] In addition, the interband dipole matrix element value is calculated to be zero at the M point, implying that the direct optical transition is forbidden at this point, as expected from symmetry considerations.[49] Meanwhile, a strong dipole matrix element value is observed at the VBM location. Therefore, the phonon-assisted indirect radiative recombination process requires the emission of phonons of wavevector $\mathbf{q} = \overrightarrow{MK}$ followed by interband optical emission at the K point.[17] Based on the bandstructure analysis, we have further investigated the luminescence intensity of indirect optical transitions in h-BN by considering the relevant electron-phonon scattering processes. Using second-order perturbation theory, the

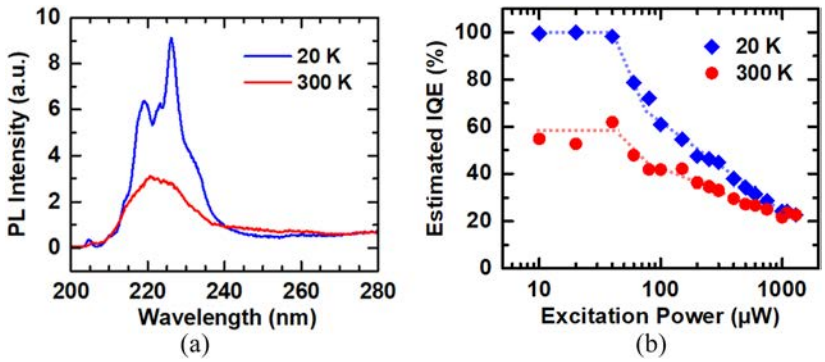

FIG. 2. (a) Photoluminescence (PL) spectra of h-BN/Ni(111) at 20 and 300 K. The same spectra in units of energy and at various excitation powers and temperatures can be found in Sec. 4 of the supplementary material. (b) Estimated internal quantum efficienc (IQE) of h-BN/Ni at various excitation powers, plotted in logarithmic scale. The dashed lines serve as a guide to the reader. This relation at additional temperatures can be also found in Sec. 4 of the supplementary material.

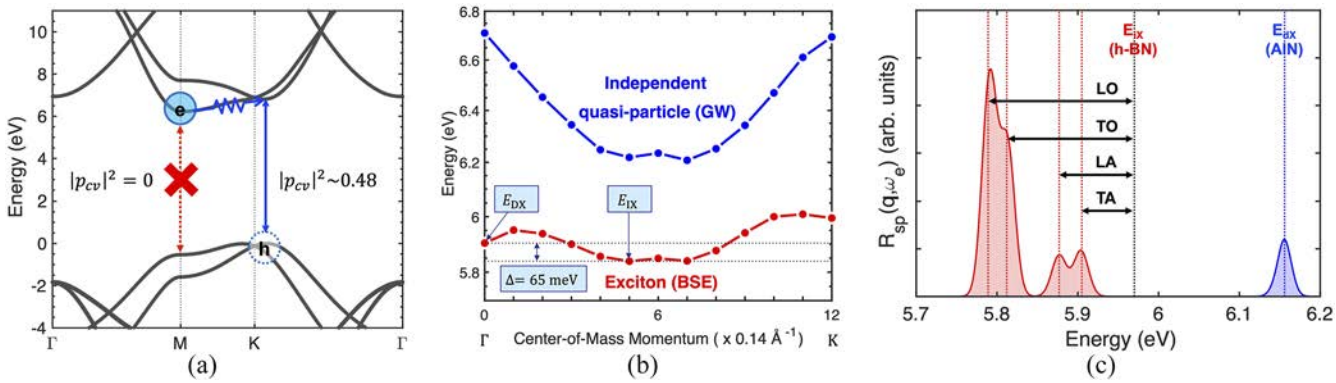

FIG. 3. (a) Quasi-particle band structure and interband dipole matrix elements of bulk h-BN. The direct optical transition at the CBM location ($\mathbf{k} = \mathrm{M}$) is dipole forbidden due to the symmetry of the crystal, whereas a strong transition dipole moment is predicted ($|p_{cv}|^2 \sim 0.48$, in atomic unit) for the VBM location ($\mathbf{k} \sim \mathbf{K}$). (b) Exciton dispersion relation of *h*-BN obtained from the Bethe-Salpeter equation (red curve) compared with the excitation energy of independent quasiparticles obtained from GW calculation (blue curve). Our calculation indicates that the lowest-energy indirect exciton state is at $q = 5q_0 \approx 0.7\ \text{Å}^{-1}$, located 65 meV below the direct exciton state. (c) The spontaneous emission spectrum of bulk h-BN and bulk AlN. The red (blue)-dashed line indicates the lowest-energy indirect (direct) exciton state of h-BN (AlN). The arrows indicate the energy of the phonon modes that contribute to the phonon-assisted emission of h-BN.

transition matrix element S for this phonon-assisted transition can be written as[23,46,50]

$$S^2 = \frac{M_{dX}^2 {M_{ephX}}^2}{\left(E_d - E_i + \hbar\omega_{ph}\right)^2}, \tag{1}$$

where M_{dX} is the direct optical transition matrix element, M_{ephX} is the exciton-phonon coupling matrix elements, E_d and E_i are the energies of direct and indirect transitions, and $\hbar\omega_{ph}$ is the phonon energy involved in the phonon-assisted transition. First, the direct optical transition matrix element (or the oscillator strength of direct excitons) can be deduced from the size of the excitons. Based on the reported values of the exciton Bohr radius $\left(a_X^{BN} = 8\ \text{Å}, a_X^{AlN} = 15\ \text{Å}\right)$[24,51] and the Wannier-Mott model that predicts $M_{dX}^2 \propto 1/a_X^3$, we can estimate that the oscillator strength of direct excitons of h-BN is approximately one order of magnitude higher than that in AlN. The strong oscillator strength of h-BN indicates exceptionally strong light–matter interactions, which has been attributed to the quasi-2D nature of excitons in h-BN.[52,53]

We have further performed density-functional perturbation theory (DFPT) calculations to analyze the electron–phonon scattering processes, which assist indirect optical transitions in h-BN. From DFPT, the electron–phonon matrix elements are define as

$$g_{mn\nu}^{\mathbf{k},\mathbf{q}} = \left\langle u_{m\mathbf{k}+\mathbf{q}} | \Delta_{\mathbf{q}\nu} v^{\mathrm{KS}} | u_{n\mathbf{k}} \right\rangle, \tag{2}$$

where $u_{n\mathbf{k}}$ is the Bloch components of electron wavefunctions for the band index n and the electron wavevector $\mathbf{k}$, and $\Delta_{\mathbf{q}\nu} v^{\mathrm{KS}}$ is the phonon-induced variation of the self-consistent potential v^{KS} with respect to the phonon wavevector $\mathbf{q}$ and the phonon branch index ν. We only consider the relevant phonon scattering processes, wherein electrons at CBM ($\mathbf{k} = \mathrm{M}$) are scattered by the phonons with momentum $\mathbf{q} = \overrightarrow{\mathrm{MK}}$ and transferred to the K point. The magnitude of the electron–phonon matrix element for each phonon branch of h-BN is summarized in Table S6.1 in Sec. 6 of the supplementary material. Several phonon branches exhibit coupling intensity of the order of a few tens of meV. In particular, the strongest electron–phonon coupling is predicted for the longitudinal optical phonon (LO), ($|g_{\mathrm{LO}}| = 111\ \text{meV}$) as typically observed for polar materials.[54,55] We also point out that for charge-neutral excitons, electron–phonon and hole-phonon coupling can compensate each other so that the exciton phonon may show less significan coupling.[56] However, since hole-phonon scattering contribution is negligible for the indirect excitons in this case, we expect that both electron–phonon matrices and exciton–phonon matrices are of similar magnitude.[57]

Furthermore, our exciton calculation predicts the flattenin of the exciton dispersion relation in h-BN, as shown in Fig. 3(b). Our calculation confirm that the lowest-energy indirect exciton state is mainly formed by the indirect electron–hole pairs near the band extrema (Fig. S6.1). In particular, the calculated energy difference between the direct and the indirect transitions is merely 65 meV, in good agreement with the experimental value of 70 meV.[48] This value is much smaller than the values of other typical indirect-gap materials, such as silicon or diamond. Thus, the sum of all energy terms in the denominator of S is still comparable with the magnitude of the electron–phonon coupling matrix for h-BN (Table S6.1). Therefore, we propose that the strong electron–phonon coupling and the fla exciton dispersion promote bright luminescence for h-BN, although it is an indirect-gap material.

We further confir strong photoemission from h-BN by directly calculating the phonon-assisted optical absorption and emission spectra of bulk h-BN. We adopted the special displacement method, where the atoms in a large supercell are displaced to incorporate the electron–phonon interactions.[58,59] In addition, we invoke the detailed balance principle to obtain the spontaneous emission rate.[60,61] Details are included in Sec. 5 of the supplementary material. Figure 3(c) shows the spontaneous emission rate of h-BN and AlN. Compared with the absorption spectrum (Fig. S6.2), the

emission peaks of h-BN are shifted to the lower-energy side of the indirect exciton state, showing the mirror symmetry between the indirect absorption and emission processes. In addition, bulk h-BN is predicted to exhibit a much higher spontaneous emission rate than bulk AlN, directly indicating its high luminescence efficiency Finally, we also point out that the relative intensity and the position of each emission peak match well with the previously reported PL spectrum.

Several other factors should be considered to explain the high luminescence efficienc of h-BN. First, nonradiative processes can compete with the radiative process and suppress the luminescence efficiency For h-BN, the radiative recombination time is experimentally proven to occur at the sub-nanosecond scale,[62–64] owing to the efficien exciton–phonon interactions. Efficien exciton–phonon interaction and a strong exciton oscillator strength, caused by extremely fla bands along the c-axis, attributed to the 2D nature of h-BN, enable very fast radiative recombination processes. Thus, for high-quality h-BN, it is fast enough to bypass many nonradiative recombination processes. In addition to the internal quantum effi ciency, the extraction efficienc is also a key performance parameter of UV LEDs. In the case of bulk AlN or Al-rich $Al_xGa_{1-x}N$ alloys, TM-polarized light emission has been considered a bottleneck in the development of high-efficienc deep UV LEDs.[65–68] Meanwhile, from polarization-resolving PL, we found that h-BN exhibits predominantly transverse electric (TE)-polarized light emission, shown in Sec. 7 of the supplementary material, which is beneficia for efficien light extraction.[46] Furthermore, the indirect bandgap of h-BN leads to a Stokes shift between the absorption and emission spectra and prevents the re-absorption of the emitted photons,[7,48] which is known to severely suppress the extraction efficienc for direct-bandgap semiconductors.[69] These factors provide unambiguous evidence that h-BN can exhibit a bright luminescence intensity, even stronger than AlN, despite the indirect nature of its bandgap.

In summary, we have demonstrated, both theoretically and experimentally, that h-BN, albeit with an indirect bandgap, exhibits remarkably high luminescence efficienc at room temperature, which is explained by strong electron–phonon coupling and excitonic effects. It was found that the Ni substrate serves as an ideal substrate for h-BN growth due to minimal lattice mismatch and optimal interfacial interactions. Moreover, the achievement of wafer-scale superior quality h-BN paves the way for their emerging applications in deep UV optoelectronics, high-frequency, and high-power electronics, as well as a broad range of nanoscale electronic and quantum devices and systems.

METHODS

Theory and computations (h-BN/substrate heterointerfaces)

All calculations were performed by employing the spin-polarized density functional theory (DFT) within a general gradient approximation (GGA) parameterized by Perdew, Burke, and Ernzerhof (PBE),[70,71] as implemented in the Vienna *ab initio* simulation package (VASP).[72,73] The electron-ion potential was described by the projected augmented wave (PAW) method,[74,75] and a kinetic energy cutoff of 520 eV was used for the plane wave expansion. All structures were relaxed until the atomic forces were less than 0.01 eV/Å, and total energies were converged to 10^{-5} eV. Models were constructed to examine the interaction of h-BN with different substrates, including (111), (115), and (110) substrates of Ni and Cu, sapphire, and quartz. Specificall for h-BN on sapphire, since sapphire would experience a high degree of nitridation under high-temperature MBE conditions, causing the formation of AlN in between sapphire and h-BN, AlN is thus expected to be the actual material interfacing with h-BN and was used as the effective substrate in the model.[27] The AlN substrate was terminated by Al to avoid any nitrogen alloying or diffusion with/to h-BN (for details, see Sec. 8 of the supplementary material). Trigonal quartz alpha with silicon exposed to h-BN was used to represent a SiO_2 substrate.[4] The models were illustrated in Fig. 1, where periodic conditions were applied. A vacuum space of >30 Å along the direction (i.e., *z*-axis) perpendicular to the h-BN sheet was used to eliminate interaction between periodic images. Given the different lattice structures and lattice constants of the substrates, different supercells were used, detailed in Sec. 8 of the supplementary material. DFT-D2 method of Grimme was used to describe Van der Waals (vdW) interaction resulting from dynamical correlations between fluctuatin polarizations of molecules.[76]

To quantitatively analyze the interaction between h-BN and different underlying substrates, the adhesion energy $\beta_{\mathrm{hBN-sub}}$ was computed,[77,78]

$$\beta_{\mathrm{hBN-sub}} = \frac{E_{\mathrm{hBN}} + E_{\mathrm{sub}} - E_{\mathrm{hBN-sub}}}{A}, \tag{3}$$

where E_{hBN}, E_{sub}, and $E_{hBN\text{-}sub}$ are the energies of the h-BN sheet, substrate slab, and the h-BN-substrate system, respectively, whereas A is the area of the interface between h-BN and the substrate. Meanwhile, the formation of N or B vacancies in h-BN on different substrates was examined, with the corresponding vacancy formation energy E_v^i calculated as

$$E_v^i = E_{\mathrm{hBN-sub}} - E_{\mathrm{hBN-sub,v}} - \mu_i, \tag{4}$$

where i denotes the type of defect (i.e., N or B) and μ_i is the chemical potential of element i. $E_{\mathrm{hBN-sub}}$ and $E_{\mathrm{hBN-sub,v}}$ are the total energies of the pristine and defective h-BN-substrate systems, respectively. More details can be found in Sec. 9 of the supplementary material.

Theory and computations (h-BN luminescence efficiency)

Electronic, optical, and phonon properties of bulk hexagonal boron nitride were calculated based on DFT and many-body perturbation theory. For DFT calculations, we used norm-conserving pseudopotentials and local density approximations (LDA) for the exchange-correlation functional,[79,80] as implemented in the Quantum Espresso package.[81] GW and Bethe-Salpeter Equation calculations were performed using the BerkeleyGW package.[82] The computational details are listed in Sec. 5 of the supplementary material.

Molecular beam epitaxial growth

The MBE growth of h-BN on Ni(111) is described in the previous work.[23] Unannealed polycrystal Ni metallic wafers from MTI Corporation, with dimensions of 2 inch square, and a thickness of

1 mm, were used as the substrate for some studies described in this work. These wafers were directly loaded from their vacuum packaging into the load lock of the MBE system without any wet processing to avoid the surface oxidation of Ni. The wafers were thermally degassed prior to transferring into the growth chamber. After being loaded into the growth chamber, the Ni wafer was ramped up to 800 °C (thermocouple temperature reading, with the real surface temperature estimated to be ~1100 °C) and maintained for 30 min to thermally desorb the surface native oxide.[83] The growths were conducted in similar conditions as the previous optimization study,[23] using a relatively low B deposition rate (<0.05 Å/s) and nitrogen-rich plasma parameters (a flo rate of 1.5 sccm with a forward power of 350 W). The growth durations were between 30 min and 1 h. Growth was conducted using a Veeco GENxplor radio frequency (RF) nitrogen plasma-assisted MBE system equipped with an e-beam evaporation source for elemental boron (99.999% purity). The boron evaporation rate was monitored with an Infico Guardian EIES controller.

Optical characterization

For PL spectroscopy, the samples were excited using a 193 nm ArF excimer laser. The emissions were spectrally resolved using a Horiba iHR550 spectrometer and a UV-sensitive Symphony II CCD detector. The measured spectra were processed using a percentile filte smoothing function for the removal of random artifact spikes captured by the CCD detector and that are unrelated to the sample. The temperature-dependent measurements were conducted with the sample inside a closed-loop helium cryostat coupled with a cryogenic temperature controller. For the comparative IQE study, the calculated integrated intensities from the power-dependent runs were cross-calibrated using the temperature-dependent run and then normalized by the maximum integrated intensity. Polarization-resolving PL consisted in collecting the in-plane emission from the sample (i.e., from the side facet) and measuring the intensity after passing it through an optical polarizer mounted on a rotation stage.

SUPPLEMENTARY MATERIAL

The supplementary material includes the synthesis of h-BN, photoluminescence properties of h-BN on Ni and other substrates, and details about *Ab initio* calculations.

ACKNOWLEDGMENTS

This work was supported by the Army Research Offic (ARO) (Grant No. W911NF-17-1-0312), National Science Foundation (NSF) (Grant Nos. DMR-1807984 and 2118809), the Blue Sky Program in the College of Engineering at the University of Michigan, and the W. M. Keck Foundation. The phonon-assisted optical spectra calculations were supported as part of the Computational Materials Sciences Program funded by the U.S. Department of Energy, Offic of Science, Basic Energy Sciences, under Award No. DE-SC0020129. The interface calculations were supported by Natural Sciences and Engineering Research Council of Canada Discovery Grant No. RGPIN-2017-05187, and the computational resource was provided by Digital Alliance of Canada. D.A.L. wishes to acknowledge financia support by the Natural Sciences and Engineering Research Council of Canada (NSERC) with Award No. PGSD3-502905-2017. W.L. was partially supported by the Kwanjeong Educational Foundation Scholarship. Y.Z. was supported by a McGill Engineering Doctoral Award (MEDA). This research used resources of the National Energy Research Scientifi Computing Center (NERSC), a U.S. Department of Energy Offic of Science User Facility located at Lawrence Berkeley National Laboratory, operated under Contract No. DE-AC02-05CH11231. Part of the work was performed at the Lurie Nanofabrication Facility (LNF) at the University of Michigan. The authors would like to thank Mr. Eric T. Reid for setting up and conducting the polarization-resolving PL measurements, Mr. Haozhi Dong for assistance with data processing of the PL measurements, and Dr. Marios Zacharias for discussions related to the indirect absorption calculation using the special displacement method. We also acknowledge Dr. Zhongrui (Jerry) Li at the Robert B. Mitchell Electron Microbeam Analysis Lab (EMAL) of the University of Michigan for assistance with the Auger electron spectroscopy (AES) experiments and data analysis, and Dr. Pilar Herrera-Fierro from the LNF for support with the tunneling atomic force microscopy (TUNA) experiment.

AUTHOR DECLARATIONS

Conflict of Interest

Some IP related to this work has been licensed to NS Nanotech, Inc., which was co-founded by Z. Mi. The University of Michigan and Mi have a financia interest in the company.

Author Contributions

David Arto Laleyan, Woncheol Lee, Ying Zhao, and Yuanpeng Wu contributed equally to this work.

David Arto Laleyan: Conceptualization (equal); Data curation (equal); Formal analysis (equal); Investigation (equal); Methodology (equal); Validation (equal); Visualization (equal); Writing – original draft (equal); Writing – review & editing (equal). **Woncheol Lee**: Conceptualization (equal); Data curation (equal); Formal analysis (equal); Investigation (equal); Methodology (equal); Project administration (equal); Software (equal); Validation (equal); Writing – original draft (equal); Writing – review & editing (equal). **Ying Zhao**: Conceptualization (equal); Data curation (equal); Formal analysis (equal); Investigation (equal); Methodology (equal); Software (equal); Supervision (equal); Validation (equal); Visualization (equal); Writing – original draft (equal); Writing – review & editing (equal). **Yuanpeng Wu**: Formal analysis (equal); Investigation (equal); Methodology (equal); Validation (equal); Writing – review & editing (equal). **Ping Wang**: Conceptualization (equal); Data curation (equal); Formal analysis (equal); Investigation (equal); Methodology (equal); Software (equal); Validation (equal); Visualization (equal); Writing – original draft (equal); Writing – review & editing (equal). **Jun Song**: Conceptualization (equal); Data curation (equal); Formal analysis (equal); Funding acquisition (equal); Investigation (equal); Methodology (equal); Project administration (equal); Resources (equal); Software (equal); Supervision (equal); Validation (equal); Visualization (equal); Writing – original draft (equal); Writing – review & editing (equal). **Emmanouil Kioupakis**: Conceptualization (equal); Data curation (equal); Formal analysis

(equal); Funding acquisition (equal); Investigation (equal); Methodology (equal); Project administration (equal); Resources (equal); Software (equal); Supervision (equal); Validation (equal); Visualization (equal); Writing – original draft (equal); Writing – review & editing (equal). **Zetian Mi**: Conceptualization (equal); Data curation (equal); Formal analysis (equal); Funding acquisition (equal); Investigation (equal); Methodology (equal); Project administration (equal); Resources (equal); Software (equal); Supervision (equal); Validation (equal); Visualization (equal); Writing – original draft (equal); Writing – review & editing (equal).

DATA AVAILABILITY

The data that support the finding of this study are available from the corresponding authors upon reasonable request.

REFERENCES

[1] A. K. Geim and I. V. Grigorieva, "Van der Waals heterostructures," Nature **499**, 419–425 (2013).
[2] E. V. Calman *et al.*, "Indirect excitons in van der Waals heterostructures at room temperature," Nat. Commun. **9**, 1895 (2018).
[3] M. Sammon and B. I. Shklovskii, "Attraction of indirect excitons in van der Waals heterostructures with three semiconducting layers," Phys. Rev. B **99**, 165403 (2019).
[4] D. A. Laleyan *et al.*, "AlN/h-BN heterostructures for Mg dopant-free deep ultraviolet photonics," Nano Lett. **17**, 3738–3743 (2017).
[5] M. Han *et al.*, "Characteristics of aluminum nitride film on hexagonal boron nitride buffer layers using various growth methods through metal organic chemical vapor deposition," J. Cryst. Growth **507**, 316–320 (2019).
[6] D. T. Thanh *et al.*, "Hexagonal boron nitride pattern embedded in AlN template layer for visible-blind ultraviolet photodetectors," Opt. Mater. Express **7**, 1463–1472 (2017).
[7] J. D. Caldwell *et al.*, "Photonics with hexagonal boron nitride," Nat. Rev. Mater. **4**, 552–567 (2019).
[8] K. Watanabe, T. Taniguchi, T. Niiyama, K. Miya, and M. Taniguchi, "Far-ultraviolet plane-emission handheld device based on hexagonal boron nitride," Nat. Photonics **3**, 591–594 (2009).
[9] M. Buonanno, D. Welch, I. Shuryak, and D. J. Brenner, "Far-UVC light (222 nm) efficientl and safely inactivates airborne human coronaviruses," Sci. Rep. **10**, 10285 (2020).
[10] D. Welch *et al.*, "Far-UVC light: A new tool to control the spread of airborne-mediated microbial diseases," Sci. Rep. **8**, 2752 (2018).
[11] H. Wang, Y. Zhao, Y. Xie, X. Ma, and X. Zhang, "Recent progress in synthesis of two-dimensional hexagonal boron nitride," J. Semicond. **38**, 031003 (2017).
[12] K. Zhang, Y. Feng, F. Wang, Z. Yang, and J. Wang, "Two dimensional hexagonal boron nitride (2D-hBN): Synthesis, properties and applications," J. Mater. Chem. C **5**, 11992–12022 (2017).
[13] T. Taniguchi and K. Watanabe, "Synthesis of high-purity boron nitride single crystals under high pressure by using Ba–BN solvent," J. Cryst. Growth **303**, 525–529 (2007).
[14] Y. Kubota, K. Watanabe, O. Tsuda, and T. Taniguchi, "Deep ultraviolet light-emitting hexagonal boron nitride synthesized at atmospheric pressure," Science **317**, 932–934 (2007).
[15] S. Liu *et al.*, "Large-scale growth of high-quality hexagonal boron nitride crystals at atmospheric pressure from an Fe–Cr flux, Cryst. Growth Des. **17**, 4932–4935 (2017).
[16] P. Wang *et al.*, "Scalable synthesis of monolayer hexagonal boron nitride on graphene with giant bandgap renormalization," Adv. Mater. **34**, 2201387 (2022).
[17] G. Cassabois, P. Valvin, and B. Gil, "Hexagonal boron nitride is an indirect bandgap semiconductor," Nat. Photonics **10**, 262–266 (2016).
[18] L. J. Martínez *et al.*, "Efficien single photon emission from a high-purity hexagonal boron nitride crystal," Phys. Rev. B **94**, 121405 (2016).
[19] A. Sajid, M. J. Ford, and J. R. Reimers, "Single-photon emitters in hexagonal boron nitride: A review of progress," Rep. Prog. Phys. **83**, 044501 (2020).
[20] T. T. Tran, K. Bray, M. J. Ford, M. Toth, and I. Aharonovich, "Quantum emission from hexagonal boron nitride monolayers," Nat. Nanotechnol. **11**, 37–41 (2016).
[21] N. Mendelson *et al.*, "Identifying carbon as the source of visible single-photon emission from hexagonal boron nitride," Nat. Mater. **20**, 321–328 (2021).
[22] K. Watanabe, T. Taniguchi, and H. Kanda, "Direct-bandgap properties and evidence for ultraviolet lasing of hexagonal boron nitride single crystal," Nat. Mater. **3**, 404–409 (2004).
[23] D. A. Laleyan *et al.*, "Effect of growth temperature on the structural and optical properties of few-layer hexagonal boron nitride by molecular beam epitaxy," Opt. Express **26**, 23031–23039 (2018).
[24] X. K. Cao, B. Clubine, J. H. Edgar, J. Y. Lin, and H. X. Jiang, "Two-dimensional excitons in three-dimensional hexagonal boron nitride," Appl. Phys. Lett. **103**, 191106 (2013).
[25] T. Q. P. Vuong *et al.*, "Deep ultraviolet emission in hexagonal boron nitride grown by high-temperature molecular beam epitaxy," 2D Mater. **4**, 021023 (2017).
[26] S.-B. Song *et al.*, "Deep-ultraviolet electroluminescence and photocurrent generation in graphene/hBN/graphene heterostructures," Nat. Commun. **12**, 7134 (2021).
[27] R. Page *et al.*, "Rotationally aligned hexagonal boron nitride on sapphire by high-temperature molecular beam epitaxy," Phys. Rev. Mater. **3**, 064001 (2019).
[28] K. Ahmed *et al.*, "Effects of sapphire nitridation and growth temperature on the epitaxial growth of hexagonal boron nitride on sapphire," Mater. Res. Express **4**, 015007 (2017).
[29] C. D. Spataru, M. H. Crawford, and A. A. Allerman, "First principles study of hBN-AlN short-period superlattice heterostructures," Appl. Phys. Lett. **114**, 011903 (2019).
[30] A.-R. Jang *et al.*, "Wafer-scale and wrinkle-free epitaxial growth of single-orientated multilayer hexagonal boron nitride on sapphire," Nano Lett. **16**, 3360–3366 (2016).
[31] J. Strand, L. Larcher, and A. L. Shluger, "Properties of intrinsic point defects and dimers in hexagonal boron nitride," J. Phys.: Condens. Matter **32**, 055706 (2019).
[32] I. H. Abidi *et al.*, "Selective defect formation in hexagonal boron nitride," Adv. Opt. Mater. **7**, 1900397 (2019).
[33] L. Weston, D. Wickramaratne, M. Mackoit, A. Alkauskas, and C. G. Van de Walle, "Native point defects and impurities in hexagonal boron nitride," Phys. Rev. B **97**, 214104 (2018).
[34] C. Attaccalite, M. Bockstedte, A. Marini, A. Rubio, and L. Wirtz, "Coupling of excitons and defect states in boron-nitride nanostructures," Phys. Rev. B **83**, 144115 (2011).
[35] J. Li *et al.*, "Nature of exciton transitions in hexagonal boron nitride," Appl. Phys. Lett. **108**, 122101 (2016).
[36] X. Z. Du, J. Li, J. Y. Lin, and H. X. Jiang, "The origin of deep-level impurity transitions in hexagonal boron nitride," Appl. Phys. Lett. **106**, 021110 (2015).
[37] X. Z. Du, J. Li, J. Y. Lin, and H. X. Jiang, "The origins of near band-edge transitions in hexagonal boron nitride epilayers," Appl. Phys. Lett. **108**, 052106 (2016).
[38] D. A. Laleyan *et al.*, "Molecular beam epitaxy and characterization of $Al_{0.6}Ga_{0.4}N$ epilayers," J. Cryst. Growth **507**, 87–92 (2019).
[39] A. H. Park *et al.*, "Efficien stress-relaxation in InGaN/GaN light-emitting diodes using carbon nanotubes," Nanoscale **7**, 15099–15105 (2015).
[40] A. Laubsch *et al.*, "Measurement of the internal quantum efficienc of InGaN quantum wells," Proc. SPIE **6486**, 64860J (2007).
[41] Y. Zhong, E. Berikaa, J. Lu, X. Yin, and S. Zhao, "Molecular beam epitaxial growth and optical characterization of AlGaN nanowires with reduced substrate temperature," AIP Adv. **10**, 025022 (2020).
[42] E. Kioupakis, P. Rinke, K. T. Delaney, and C. G. Van de Walle, "Indirect Auger recombination as a cause of efficienc droop in nitride light-emitting diodes," Appl. Phys. Lett. **98**, 161107 (2011).
[43] E. Kioupakis, Q. Yan, and C. G. Van de Walle, "Interplay of polarization field and Auger recombination in the efficienc droop of nitride light-emitting diodes," Appl. Phys. Lett. **101**, 231107 (2012).

[44]M.-H. Kim *et al.*, "Origin of efficienc droop in GaN-based light-emitting diodes," Appl. Phys. Lett. **91**, 183507 (2007).
[45]D. S. Meyaard *et al.*, "Identifying the cause of the efficienc droop in GaInN light-emitting diodes by correlating the onset of high injection with the onset of the efficienc droop," Appl. Phys. Lett. **102**, 251114 (2013).
[46]K. A. Mengle and E. Kioupakis, "Impact of the stacking sequence on the bandgap and luminescence properties of bulk, bilayer, and monolayer hexagonal boron nitride," APL Mater. **7**, 021106 (2019).
[47]T. Shen *et al.*, "Influenc of high-energy local orbitals and electron-phonon interactions on the band gaps and optical absorption spectra of hexagonal boron nitride," Phys. Rev. B **102**, 045117 (2020).
[48]L. Schué *et al.*, "Bright luminescence from indirect and strongly bound excitons in h-BN," Phys. Rev. Lett. **122**, 067401 (2019).
[49]B. Arnaud, S. Lebègue, P. Rabiller, and M. Alouani, "Huge excitonic effects in layered hexagonal boron nitride," Phys. Rev. Lett. **96**, 026402 (2006).
[50]S. Roux *et al.*, "Radiative lifetime of free excitons in hexagonal boron nitride," Phys. Rev. B **104**, L161203 (2021).
[51]R. Ishii, M. Funato, and Y. Kawakami, "Huge electron-hole exchange interaction in aluminum nitride," Phys. Rev. B **87**, 161204 (2013).
[52]B. Huang, X. K. Cao, H. X. Jiang, J. Y. Lin, and S.-H. Wei, "Origin of the significantl enhanced optical transitions in layered boron nitride," Phys. Rev. B **86**, 155202 (2012).
[53]C. Elias *et al.*, "Flat bands and giant light-matter interaction in hexagonal boron nitride," Phys. Rev. Lett. **127**, 137401 (2021).
[54]K. Krishnaswamy, B. Himmetoglu, Y. Kang, A. Janotti, and C. G. Van de Walle, "First-principles analysis of electron transport in $BaSnO_3$," Phys. Rev. B **95**, 205202 (2017).
[55]Y. Kang, H. Peelaers, and C. G. Van de Walle, "First-principles study of electron-phonon interactions and transport in anatase TiO_2," Phys. Rev. B **100**, 121113 (2019).
[56]A. Chernikov, V. Bornwasser, M. Koch, S. Chatterjee, C. N. Böttge, T. Feldtmann, M. Kira, S. W. Koch, T. Wassner, S. Lautenschläger, B. K. Meyer, and M. Eickhoff, "Phonon-assisted luminescence of polar semiconductors: Fröhlich coupling versus deformation-potential scattering," Phys. Rev. B **85**, 035201 (2012).
[57]Zhang, X.-W., Xie, K., Wang, E.-G., Cao, T. and Li, X.-Z., "Phonon-mediated exciton relaxation in two-dimensional semiconductors: Selection rules and relaxation pathways," arXiv:211008873 Cond-Mat (2021).
[58]M. Zacharias and F. Giustino, "One-shot calculation of temperature-dependent optical spectra and phonon-induced band-gap renormalization," Phys. Rev. B **94**, 075125 (2016).
[59]M. Zacharias and F. Giustino, "Theory of the special displacement method for electronic structure calculations at finit temperature," Phys. Rev. Res. **2**, 013357 (2020).
[60]F. Paleari, H. P. C. Miranda, and L. Wirtz, "Exciton-phonon coupling in the ultraviolet absorption and emission spectra of bulk hexagonal boron nitride," Phys. Rev. Lett. **122**, 187401 (2019).
[61]H. B. Bebb and E. W. Williams, "Chapter 4 photoluminescence I: Theory," in *Semiconductors and Semimetals*, edited by R. K. Willardson and A. C. Beer (Elsevier, 1972), Vol. 8, pp. 181–320.
[62]K. Watanabe, T. Taniguchi, T. Kuroda, O. Tsuda, and H. Kanda, "Time-resolved photoluminescence in band-edge region of hexagonal boron nitride single crystals," Diamond Relat. Mater. **17**, 830–832 (2008).
[63]G. Cassabois, P. Valvin, and B. Gil, "Intervalley scattering in hexagonal boron nitride," Phys. Rev. B **93**, 035207 (2016).
[64]S. F. Chichibu, Y. Ishikawa, H. Kominami, and K. Hara, "Nearly temperature-independent ultraviolet light emission intensity of indirect excitons in hexagonal BN microcrystals," J. Appl. Phys. **123**, 065104 (2018).
[65]J. Zhang, H. Zhao, and N. Tansu, "Effect of crystal-fiel split-off hole and heavy-hole bands crossover on gain characteristics of high Al-content AlGaN quantum well lasers," Appl. Phys. Lett. **97**, 111105 (2010).
[66]K. B. Nam, J. Li, M. L. Nakarmi, J. Y. Lin, and H. X. Jiang, "Unique optical properties of AlGaN alloys and related ultraviolet emitters," Appl. Phys. Lett. **84**, 5264–5266 (2004).
[67]Y. Taniyasu, M. Kasu, and T. Makimoto, "Radiation and polarization properties of free-exciton emission from AlN (0001) surface," Appl. Phys. Lett. **90**, 261911 (2007).
[68]R. G. Banal, M. Funato, and Y. Kawakami, "Optical anisotropy in [0001]-oriented $Al_xGa_{1-x}N$/AlN quantum wells ($x > 0.69$)," Phys. Rev. B **79**, 121308 (2009).
[69]B. Sermage and M. Voos, "Reabsorption of the excitonic luminescence in direct band gap semiconductors," Phys. Rev. B **15**, 3935–3946 (1977).
[70]J. P. Perdew, K. Burke, and M. Ernzerhof, "Generalized gradient approximation made simple," Phys. Rev. Lett. **77**, 3865–3868 (1996).
[71]J. P. Perdew, K. Burke, and M. Ernzerhof, "Generalized gradient approximation made simple [Phys. Rev. Lett. 77, 3865 (1996)]," Phys. Rev. Lett. **78**, 1396 (1997).
[72]G. Kresse and J. Furthmüller, "Efficien iterative schemes for *ab initio* total-energy calculations using a plane-wave basis set," Phys. Rev. B **54**, 11169–11186 (1996).
[73]G. Kresse and J. Furthmüller, "Efficienc of ab-initio total energy calculations for metals and semiconductors using a plane-wave basis set," Comput. Mater. Sci. **6**, 15–50 (1996).
[74]G. Kresse and D. Joubert, "From ultrasoft pseudopotentials to the projector augmented-wave method," Phys. Rev. B **59**, 1758–1775 (1999).
[75]P. E. Blöchl, "Projector augmented-wave method," Phys. Rev. B **50**, 17953–17979 (1994).
[76]S. Grimme, "Semiempirical GGA-type density functional constructed with a long-range dispersion correction," J. Comput. Chem. **27**, 1787–1799 (2006).
[77]Y. Han *et al.*, "Surface energies, adhesion energies, and exfoliation energies relevant to copper-graphene and copper-graphite systems," Surf. Sci. **685**, 48–58 (2019).
[78]D. E. Jiang and E. A. Carter, "First-principles study of the interfacial adhesion between SiO_2 and $MoSi_2$," Phys. Rev. B **72**, 165410 (2005).
[79]D. M. Ceperley and B. J. Alder, "Ground state of the electron gas by a stochastic method," Phys. Rev. Lett. **45**, 566–569 (1980).
[80]J. P. Perdew and A. Zunger, "Self-interaction correction to density-functional approximations for many-electron systems," Phys. Rev. B **23**, 5048–5079 (1981).
[81]P. Giannozzi *et al.*, "Advanced capabilities for materials modelling with Quantum ESPRESSO," J. Phys.: Condens. Matter **29**, 465901 (2017).
[82]J. Deslippe *et al.*, "BerkeleyGW: A massively parallel computer package for the calculation of the quasiparticle and optical properties of materials and nanostructures," Comput. Phys. Commun. **183**, 1269–1289 (2012).
[83]C. L. Tsai, Y. Kobayashi, T. Akasaka, and M. Kasu, "Molecular beam epitaxial growth of hexagonal boron nitride on Ni(1 1 1) substrate," J. Cryst. Growth **311**, 3054–3057 (2009).